ORIGINAL ARTICLE

mRNA m⁵C inhibits adipogenesis and promotes myogenesis by respectively facilitating *YBX2* and *SMO* mRNA export in ALYREF-m⁵C manner

Youhua Liu[1,2,3,4] · Ying Yang[5,6,7] · Ruifan Wu[1,2,3,4] · Chun-chun Gao[5,6,7] · Xing Liao[1,2,3,4] · Xiao Han[5,6,7] · Botao Zeng[1,2,3,4] · Chaoqun Huang[1,2,3,4] · Yaojun Luo[1,2,3,4] · Yuxi Liu[1,2,3,4] · Yushi Chen[1,2,3,4] · Wei Chen[1,2,3,4] · Jiaqi Liu[1,2,3,4] · Qin Jiang[1,2,3,4] · Yuanling Zhao[1,2,3,4] · Zhen Bi[1,2,3,4] · Guanqun Guo[1,2,3,4] · Yongxi Yao[1,2,3,4] · Yun Xiang[8] · Xiaojun Zhang[8] · Teresa G. Valencak[1] · Yizhen Wang[1,2,3,4] · Xinxia Wang[1,2,3,4]

Abstract

Although 5-methylcytosine (m⁵C) has been identified as a novel and abundant mRNA modification and associated with energy metabolism, its regulation function in adipose tissue and skeletal muscle is still limited. This study aimed at investigating the effect of mRNA m⁵C on adipogenesis and myogenesis using Jinhua pigs (J), Yorkshire pigs (Y) and their hybrids Yorkshire–Jinhua pigs (YJ). We found that Y grow faster than J and YJ, while fatness-related characteristics observed in Y were lower than those of J and YJ. Besides, total mRNA m⁵C levels and expression rates of NSUN2 were higher both in backfat layer (BL) and *longissimus dorsi* muscle (LDM) of Y compared to J and YJ, suggesting that higher mRNA m⁵C levels positively correlate with lower fat and higher muscle mass. RNA bisulfite sequencing profiling of m⁵C revealed tissue-specific and dynamic features in pigs. Functionally, hyper-methylated m⁵C-containing genes were enriched in pathways linked to impaired adipogenesis and enhanced myogenesis. In in vitro, m⁵C inhibited lipid accumulation and promoted myogenic differentiation. Furthermore, *YBX2* and *SMO* were identified as m⁵C targets. Mechanistically, *YBX2* and *SMO* mRNAs with m⁵C modification were recognized and exported into the cytoplasm from the nucleus by ALYREF, thus leading to increased YBX2 and SMO protein expression and thereby inhibiting adipogenesis and promoting myogenesis, respectively. Our work uncovered the critical role of mRNA m⁵C in regulating adipogenesis and myogenesis via ALYREF-m⁵C-*YBX2* and ALYREF-m⁵C-*SMO* manners, providing a potential therapeutic target in the prevention and treatment of obesity, skeletal muscle dysfunction and metabolic disorder diseases.

Keywords Adipogenesis · Myogenesis · m⁵C modification · YBX2 · SMO · ALYREF

✉ Xinxia Wang
xinxiawang@zju.edu.cn

[1] College of Animal Sciences, Zhejiang University, Hangzhou, Zhejiang, China

[2] Key Laboratory of Animal Nutrition and Feed Sciences, Ministry of Agriculture, Hangzhou, China

[3] Laboratory of Molecular Animal Nutrition (Zhejiang University), Ministry of Education, Hangzhou, China

[4] Key Laboratory of Animal Feed and Nutrition of Zhejiang Province, Hangzhou, Zhejiang, China

[5] CAS Key Laboratory of Genomic and Precision Medicine, Collaborative Innovation Center of Genetics and Development, College of Future Technology, Beijing Institute of Genomics, Chinese Academy of Sciences, Beijing, China

[6] China National Center for Bioinformation, Hangzhou, China

[7] Institute of Stem Cell and Regeneration, Chinese Academy of Sciences, Beijing, China

[8] Jinhua Academy of Agricultural Sciences, Jinhua, China

Introduction

Obesity, characterized by excessive deposition of adipose tissue, has emerged as a global public health issue which substantially increases the risk of metabolic diseases, such as type 2 diabetes mellitus, cardiovascular diseases and non-alcoholic fatty liver disease [1]. Adipose tissue is essential as energy storage while skeletal muscle is the energy burning "machinery" [2]. Skeletal muscle can account for ~ 40% of adult human body weight, and impaired myogenesis can cause muscular dystrophies and disrupted muscle regeneration, leading to physical frailty and even severe metabolic disorders [3, 4]. Several studies have demonstrated that adipose tissue is associated with skeletal muscle function and that they play a critical role in the dynamic regulation of metabolic activity and metabolic health [1, 5]. Thus, a deeper understanding of the mechanisms behind adipose and muscle development is both timely and relevant.

Numerous studies have demonstrated that RNA modifications, such as N^6-methyladenosine (m^6A), could serve as novel epigenetic marker with profound significance in regulating adipogenesis and myogenesis via modulating RNA metabolism [6, 7]. Recently, 5-methylcytosine (m^5C) has been identified as another new internal mRNA modification [8]. m^5C modification can be reversibly regulated by its methyltransferases ("writers") and demethylases ("erasers") [8–10]. Functionally, mRNA m^5C modification was reported to play a critical role in the adaptation to high temperature, in ovarian germ line stem cell development, in tumorigenesis and maternal-to-zygotic transition, also known as embryonic genome activation [11–15]. Although the role of mRNA m^5C in adipogenesis has been previously reported, the regulatory mechanism of m^5C in adipose tissue and muscle development is still limited.

On the basis of their anatomical, physiological and genomic similarities with humans, pigs have served as ideal biomedical model system to study organ development and disease progression for decades before [16]. For example, pigs are increasingly recruited as models for research on obesity and diabetes mellitus [17]. The Jinhua pig (J), a typical fat-type breed characterized by its black head and tail, high backfat layer and body fat ratio, low growth rate and less lean mass, is one of the local, popular breeds in China [18–20]. In contrast, the Yorkshire pigs (Y), as a traditional lean-type breed originating from the United States, have less fat content, higher rapid growth ratio and more muscle mass than J [21, 22]. Here, we used Jinhua pigs, Yorkshire pigs and their hybrids Yorkshire–Jinhua pigs (YJ) to explore the role of mRNA m^5C in adipose tissue and skeletal muscle development. RNA bisulfite sequencing (RNA-BisSeq) in tissues (adipose tissue and skeletal muscle) and in vitro studies demonstrated that m^5C negatively regulates adipogenesis and positively affects myogenesis. We also performed RNA-BisSeq of primary cells isolated from pig adipose tissue and skeletal muscle, and Y-box-binding protein 2 (YBX2) and smoothened (SMO) were screened out as m^5C targets by combining RNA-BisSeq from both tissue and cell data. Mechanistically, YBX2/SMO with higher m^5C were recognized and exported to cytoplasm from the nucleus by the Aly/REF export factor (ALYREF), leading to increased YBX2/SMO protein expression, thereby inhibiting adipogenesis and promoting myogenesis. Our findings reveal a regulatory mechanism of mRNA m^5C-mediated impaired adipogenesis and advantaged myogenesis in pigs and provide an important resource for studying the function of the mRNA modification during the development of obesity, skeletal muscle dysfunction and diseases caused by metabolic disorders.

Materials and methods

Animals and tissue collection

A total of 4 Jinhua pigs (male), 4 Yorkshire pigs (male) and 4 Yorkshire–Jinhua pigs (male) were humanely killed at the age of 6 months, and adipose tissue (backfat layer, BL) and skeletal muscle samples (*longissimus dorsi* muscles, LDM) from the three breeds were rapidly removed from each carcass, immediately frozen in liquid nitrogen, and stored at − 80 °C until RNA extraction.

Plasmid construction, siRNA, adenovirus production and cell transfection

For NOP2/Sun RNA methyltransferase 2 (NSUN2) and ALYREF recombinant adenovirus construction, the porcine NSUN2 and ALYREF were cloned into the pDC315-EGFP vector (Hanbio), respectively. shRNA sequences (GenePharma) were cloned into the pDC311-U6-MCMV-EGFP vector (Hanbio). The siRNA (GenePharma) and plasmid transfections were performed using Lipofectamine RNAiMAX (Invitrogen), Lipofectamine 2000 (Invitrogen) or EZ Trans (Life-iLab, China), according to the manufacturers' instructions. The target sequences for shRNA and siRNA are listed in Table S1.

Cell isolation and cell culture

Porcine subcutaneous fat pre-adipocytes (PFs) and muscle satellite cells (SCs) were isolated from subcutaneous adipose tissue and *Longissimus dorsi* muscle of 5-day-old Duroc–Landrace–Yorkshire piglets under sterile conditions,

respectively [19, 23]. Cells were cultured in high-glucose Dulbecco's modified Eagle's medium (DMEM, Thermo Fisher Scientific, Waltham, MA, USA) or DMEM/F12 medium containing 10% fetal bovine serum (Thermo Fisher Scientific) and 1% penicillin–streptomycin in the cell culture dish (NEST Biotechnology, Wuxi, China). After 2 days post confluence of cells, adipocyte differentiation was induced with adipogenic differentiation medium (containing 0.5 mM IBMX, 1 μM dexamethasone and 10 μg/mL insulin). After 2 days, the medium was replaced with a maintenance medium (containing 10% 10 μg/mL insulin) to allow for adipogenic differentiation. Cell culture and myogenic differentiation of pig SCs were performed as previously described with some modifications [24]. Briefly, when SCs become 90–100% confluent, myogenic differentiation were induced with DMEM/F12 medium containing 2% horse serum and 1% penicillin–streptomycin (Thermo Fisher Scientific). The differentiation medium was changed every 24 h, and myogenic differentiation was induced for 4–6 days.

Quantitative real-time PCR (qPCR) analysis

Total RNA from cells or tissues were extracted using TRIzol reagent (Thermo Fisher Scientific) and reverse-transcribed into cDNA using M-MLV reverse transcriptase (Thermo Fisher Scientific). qPCR was performed using the SYBR Green PCR Master Mix (Sigma-Aldrich, St. Louis, MO, USA) with the ABI Step-One Plus™ Real-Time PCR System (Thermo Fisher Scientific). The data were analyzed following the $2^{-\Delta\Delta Ct}$ method. The primer sequences are presented in Table S2.

Oil red O staining

The differentiated PFs were washed with 1 × PBS twice and fixed in 10% formalin at room temperature for 1 h. Cells were incubated in 60% isopropanol for 5 min at room temperature and then allowed to dry completely. The cells were then stained with the Oil Red O working solution (Solarbio Science and Technology Co., Ltd., Beijing, China) at room temperature for 10 min followed by 3 rinses in 1 × PBS before imaging. For quantification, Oil Red O-stained lipids were eluted in 100% isopropanol for 5 min at room temperature and absorbance was measured at 510 nm.

Bisulfite conversion of RNA, RNA-BisSeq library construction and sequencing

RNA bisulfite conversion was performed as previously described [8]. In brief, 1 μg mRNAs along with 5 ng dihydrofolate reductase (*Dhfr*) RNA as methylation conversion control were fragmented into ~200-nucleotide fragments by RNA Fragmentation Reagent (Thermo Fisher Scientific).

The fragmented RNA was re-suspended in 100 μl bisulfite solution (pH 5.1), which is a 100:1 mixture of 40% sodium bisulfite (Sigma-Aldrich) and 600 μM hydroquinone (Sigma-Aldrich) and was subjected to heat incubation at 75 °C for 4 h. The reaction mixture was desalted with Nanoseq with a 3 K omega 500/pk centrifuge (Pall Corporation, New York, USA), and then desulfonated by incubation with an equal volume of 1 M Tris (pH 9.0) at 75 °C for 1 h. After ethanol precipitation, the RNAs were re-suspended in 10 μl RNase-free water and used for library construction. cDNA libraries were constructed using the KAPA Stranded mRNA-Seq Kit (Roche, Shanghai, China). Reverse transcription was carried out using ACT random hexamers and Superscript III Reverse Transcriptase (Thermo Fisher Scientific) according to the manufacturer's instructions. Sequencing was performed on an Illumina HiSeq2500 instrument with paired end 150 bp read length.

Methylated RNA immunoprecipitation real-time PCR (meRIP-qPCR)

m⁵C meRIP-qPCR was performed as previously described with some modifications [14]. Briefly, around 2 μg mRNAs were randomly fragmented into 200–300 nt fragments by fragmentation buffer (Thermo Fisher Scientific). The fragmented mRNAs were precipitated with ethanol for following reaction. One-tenth of the fragmented mRNAs were saved as input control. 4 μg anti-m⁵C antibody (Epigentek, Farmingdale, USA) or IgG antibody (ABclonal Biotechnology Co., Ltd, Wuhan, China) was incubated with 40 μl Dynabeads Protein A (Thermo Fisher Scientific) in 300 μl IP buffer (10 mM Tris–HCl pH 7.5, 150 mM NaCl, 0.05% Triton X (*v/v*)) for 2 h at 4 °C followed by 3 rinses with 500 μl IP buffer, then the fragmented mRNAs were incubated with the prepared antibody beads at 4 °C overnight in 300 μl IP buffer. The mRNA–antibody beads complexes were washed three times with 500 μl IP buffer and then incubated in 300 μl elution buffer (5 mM Tris–HCl pH 7.5, 1 mM EDTA, 0.05% SDS, and 80 μg proteinase K) for 1 h at 50 °C, following ethanol precipitation. The eluted mRNAs and input control mRNAs were reverse-transcribed with random hexamers, and m⁵C enrichment was determined by qPCR. The data were analyzed following the $2^{-\Delta\Delta Ct}$ method, and the relative enrichment of m⁵C in each sample was calculated by normalizing to input. The primers were listed in Table S2.

m⁵C dot blots

For m⁵C dot blots, RNAs were denatured at 65 °C for 5 min. Samples were spotted on hybond-N + membrane (GE Healthcare, Chicago, USA). After UV crosslinking, the membrane was washed with PBST buffer, blocked with 5% non-fat milk and incubated with anti-m⁵C antibody
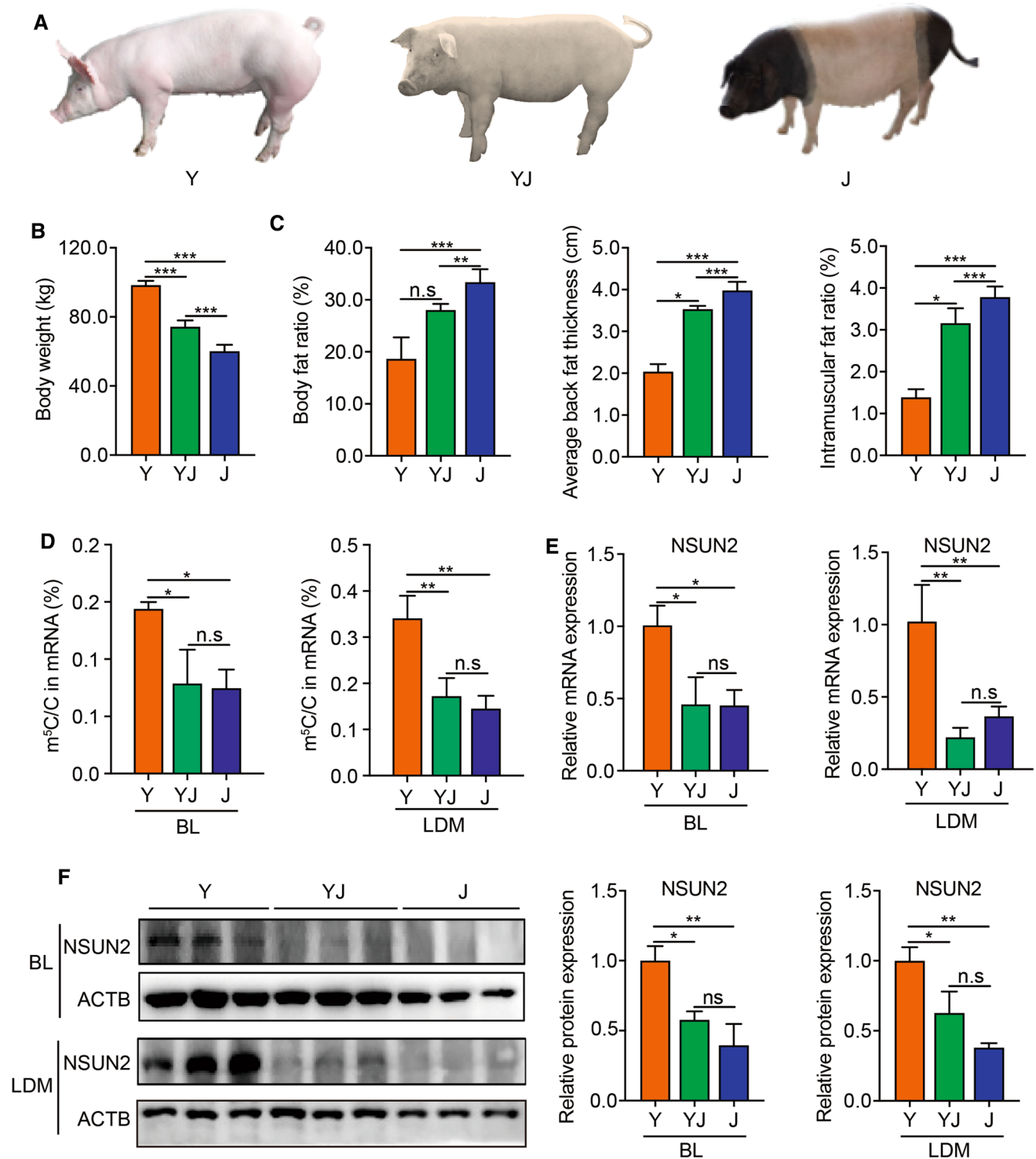
Fig. 1 Phenotypes of three pig breeds. **A** Photos of Yorkshire pigs (Y), Yorkshire×Jinhua pigs (YJ) and Jinhua pigs (J). **B** Body weights in Y, YJ and J at 180 days. Error bars, means±S.D., $n=4$. **C** Body fat ratio, average back fat thickness, intramuscular fat ratio in Y, YJ and J at 180 days of age. Error bars, means±S.D., $n=4$. **D** HPLC–MS/MS quantification of m^5C/C in mRNA of backfat layer (BL) and *longissimus dorsi muscle* (LDM) in Y, YJ and J. Error bars, means±S.D., $n=3$. **E** qPCR analysis of *NSUN2* expression in BL and LDM in Y, YJ and J at 180 days of age. 18S rRNA served as an internal RNA control. Error bars, means±S.D., $n=3$. **F** Western blotting of NSUN2 expression in BL and LDM in Y, YJ and J at 180 days of age. ACTB was used as a loading control. Error bars, means±S.D., $n=3$. The P values were determined using one-way ANOVA. *$P<0.05$ **$P<0.01$, ***$P<0.001$
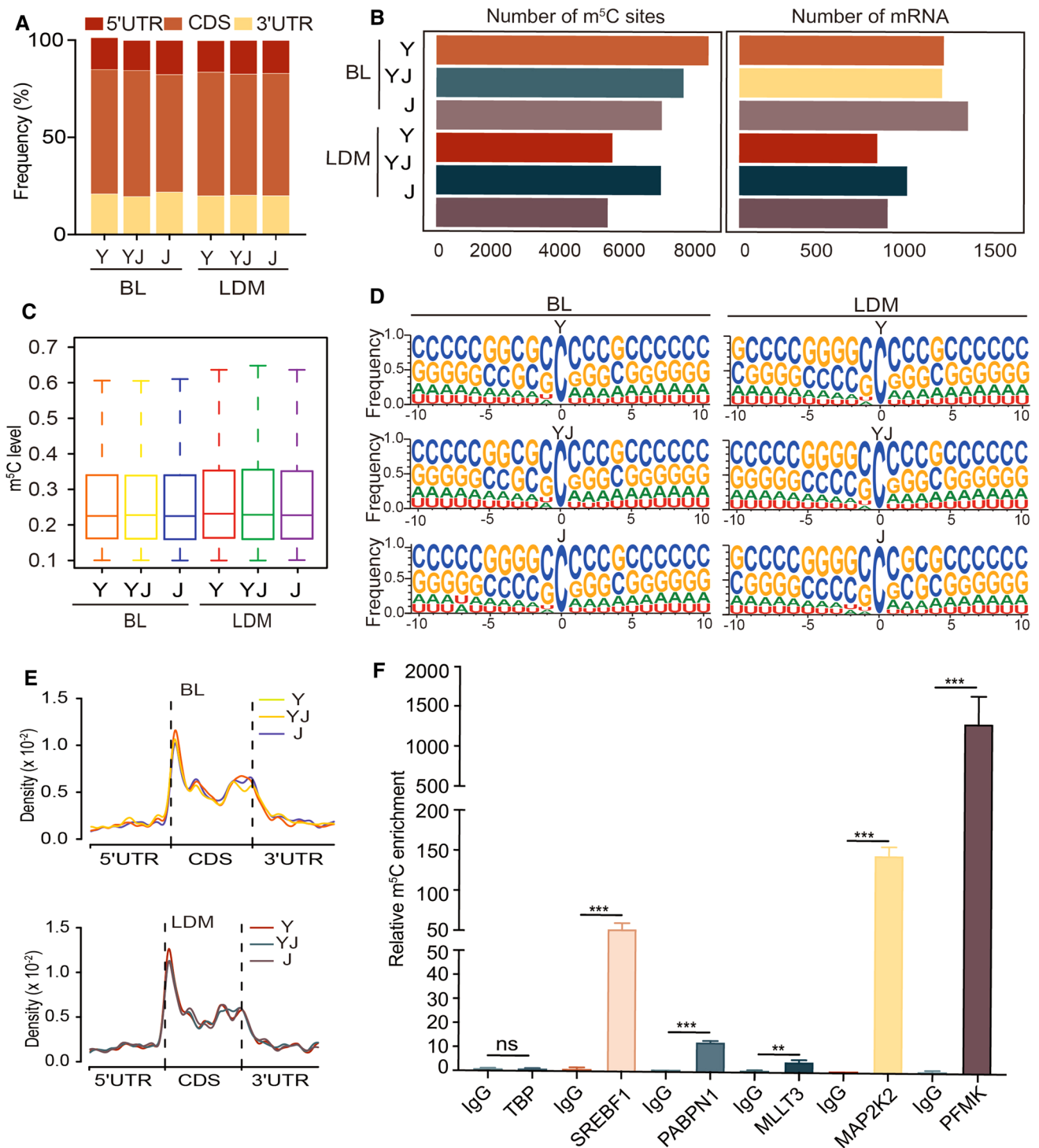
Fig. 2 Distribution of mRNA m^{5}C in BL and LDM from three different pig breeds. **A** Transcriptome-wide distribution of mRNA m^{5}C sites. The bar chart shows the percentages of m^{5}C sites within distinct mRNA regions: the 5'UTR, the CDS and the 3'UTR. **B** Bar charts showing the numbers of m^{5}C sites (left) and m^{5}C-modified mRNAs (right) in BL and LDM from Y, YJ and J. **C** Boxplots showing the overall distributions of mRNA m^{5}C levels in BL and LDM from Y, YJ and J. **D** Sequence frequency logo for the sequences proximal to mRNA m^{5}C sites. **E** The m^{5}C distributions pattern within mRNA in different regions. **F** m^{5}C-RIP-qPCR analysis of representative m^{5}C-modified genes. *TBP* served as an unmodified negative control. Error bars, means ± S.D., $n = 3$. The *P* values were determined using Student's *t* tests. *$P < 0.05$ **$P < 0.01$, ***$P < 0.001$
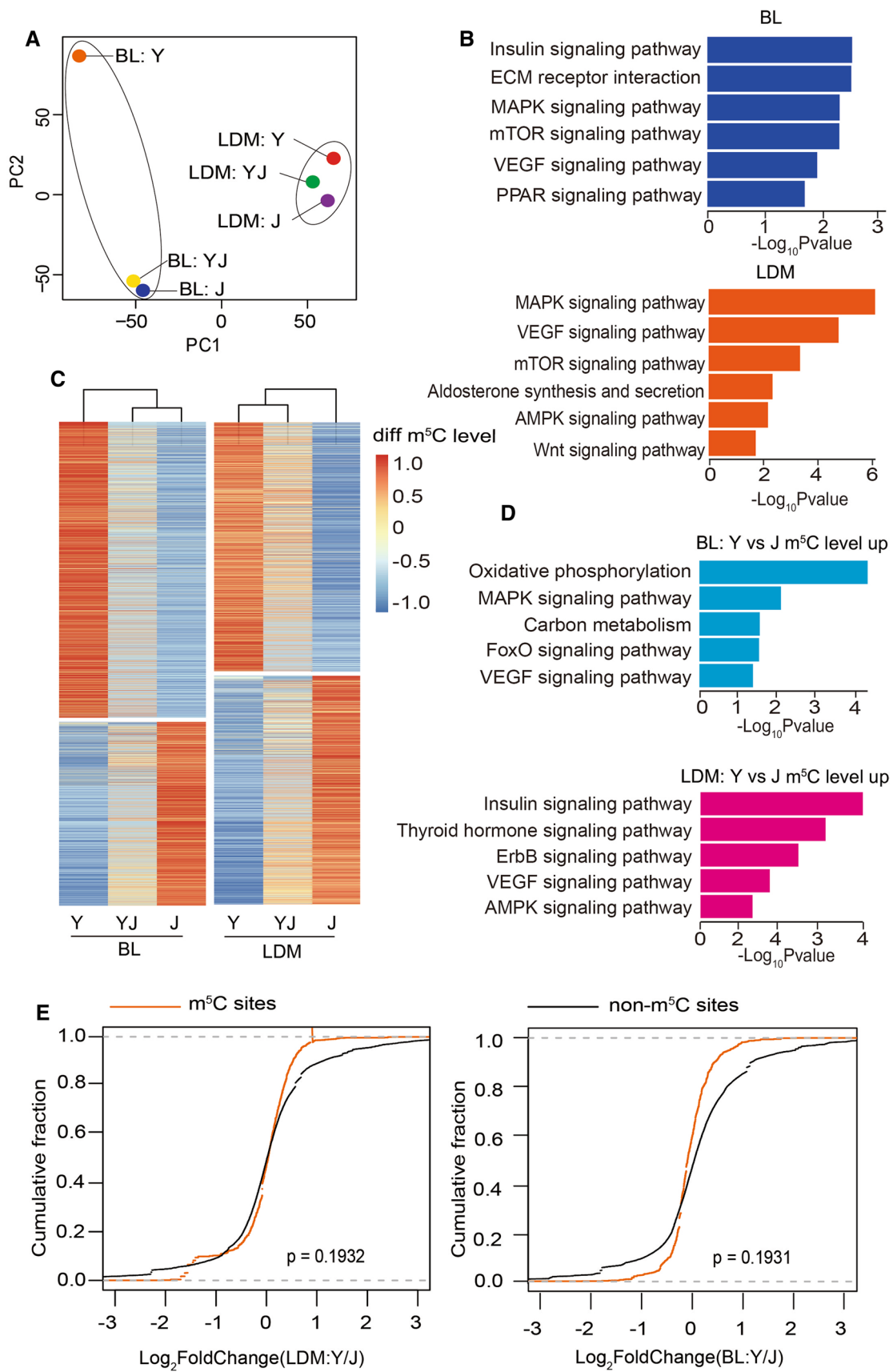
◀**Fig. 3** Hypermethylated m⁵C in BL and LDM strongly relate to fatness/growth-related phenotypes. **A** PCA analysis of m⁵C in BL and LDM from Y and YJ. **B** Bar plot showing the result of KEGG pathway analysis of m⁵C-modified mRNAs in BL and LDM (all m⁵C-modified mRNAs combined from Y, YJ and J). **C** Heatmap and cluster analysis of differentially m⁵C-modified sites (|Y-J|> 0.05) in BL and LDM from Y, YJ, and J. **D** Bar plot showing the result of KEGG pathway analysis of mRNAs with hypermethylation in BL and LDM of Y compared with J. **E** Cumulative distribution analysis of the expression level changes in mRNAs with or without m⁵C modification

overnight at 4 °C. Then, the secondary antibody was incubated at room temperature for 1 h. The membrane was visualized using chemiluminescence (ECL Plus detection system). Primary antibodies are listed in Table S3.

High-performance liquid chromatography–tandem mass spectrometry (HPLC–MS/MS)

100–200 ng of mRNAs was digested by nuclease P1 (2U) in 25 µl of buffer containing 10 mM of NH_4OAc (pH = 5.3) at 42 °C for 2 h, followed by the addition of NH_4HCO_3 (1 M, 3 µl, freshly made) and 0.5 U alkaline phosphatase with incubation at 37 °C for 2 h. Then, the sample was diluted to 50 µl and filtered (0.22 µm pore size, 4 mm diameter, Millipore), and 5 µl of the solution was injected into HPLC–MS/MS. Nucleosides were separated by reverse-phase ultra-performance liquid chromatography on a C18 column with on-line MS detection using an Agilent 6410 QQQ triple–quadrupole LC mass spectrometer in positive electrospray ionization mode. The nucleosides were quantified using the nucleoside to base ion mass transitions of 258–126 (m⁵C) and 244–112 (rC). Quantification was performed in comparison with the standard curve obtained from pure nucleoside standards running on the same batch of samples. The ratio of m⁵C to C was calculated based on the calibrated concentrations.

ALREF RNA Immunoprecipitation (RIP) assay

Flag-ALYREF overexpressing cell pellets were re-suspended with two volumes of lysis buffer (150 mM KCl, 10 mM HEPES pH 7.6, 2 mM EDTA, 0.5% NP-40, 0.5 mM DTT, 1:100 protease inhibitor cocktail, 400 U/ml RNase inhibitor), and incubated at 4 °C for 30 min while rotating. Then, the lysate was centrifuged at 12,000*g* for 20 min and mixed with M2 beads (Sigma-Aldrich) containing 600 µl NT2 buffer (200 mM NaCl, 50 mM HEPES pH 7.6, 2 mM EDTA, 0.05% NP-40, 0.5 mM DTT, 200 U/ml RNase inhibitor) and incubated at 4 °C for 4 h with rotation. After washing three times with NT2 buffer, the beads were digested with 200 µl pre-heated (20 min at 50 °C) proteinase K solution (4 mg/

ml) for 40 min at 50 °C in rotation at 2000 rpm/min. After centrifugation at top speed for 5 min, the supernatant was transferred and RNAs were extracted with an equal volume of acid–phenol:chloroform, pH 4.5 (Thermo Fisher Scientific). The RNAs were used for qPCR analysis.

Bioinformatic analysis

Raw reads were cleaned using Trimmomatic software [25]. For RNA-seq, the cleaned reads were mapped against the *Sus scrofa* genome (Sus scrofa11.1) with TopHat2 (version 2.0.13) [26]. The number of reads mapped to each ensemble gene was counted using the HTSeq software. FPKM was computed as the number of reads mapped per kilobase in the exon model per million mapped reads for each gene. mRNAs with FPKM ≥ 1 were regarded as expressing genes. For RNA-BisSeq, the cleaned reads were mapped to Sus scrofa11.1 by meRanTK (version 1.2.0). Only sites with a coverage depth ≥ 30, methylation level ≥ 0.1 and methylated cytosine depth ≥ 5 were considered credible. Only overlapping m⁵C sites between two replicates were used for the following analyses. The differences in m⁵C site level that were greater than 5% between two samples were considered increased or decreased m⁵C site methylations. The m⁵C sites were annotated by BEDTools' intersectBed. To acquire the sequence preference proximal to m⁵C sites, 21 nt sequences centering to each m⁵C site were extracted with Bedtools, and logo plots were generated with ggseqlogo. Gene ontology (GO) and KEGG pathway analyses were performed using the DAVID bioinformatics database.

Statistical analysis

All bioinformatics-related statistical analyses were performed using the R package for statistical computing. For experimental quantification, the unpaired t test in GraphPad Prism 6 software was applied, and error bars are given based on standard deviation of the mean (SD) (unless stated otherwise). $P < 0.05$ is considered as statistically significant.

Results

Phenotypes of three pig breeds

Here, we hybridized Yorkshire and Jinhua pigs and constructed an intermediate-type breed named Yorkshire–Jinhua pigs (YJ) (Fig. 1A). A total of 12 pigs (4 per breed) at an age of 180 days were randomly chosen to measure fatness/growth-related phenotypes. The body weights of Y were significantly higher than J, and YJ were just intermediate between Y and J (Fig. 1B), indicating that Y grow faster
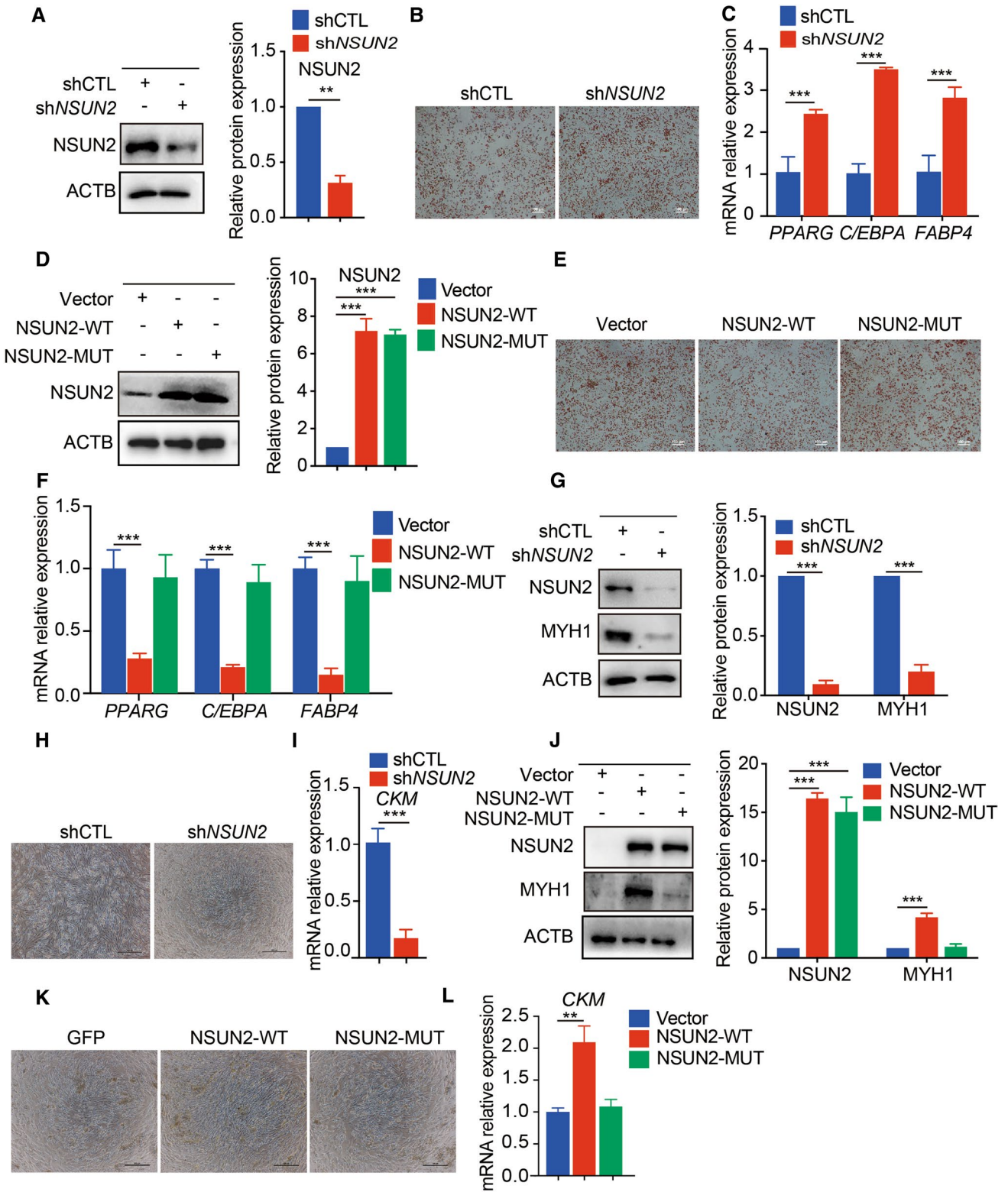
◄Fig. 4 m^{5}C inhibited adipogenesis in PFs and promoted myogenesis in SCs. **A** Western blot analysis in porcine subcutaneous fat preadipocytes (PFs) transfected with shCTL and sh*NSUN2* adenovirus. ACTB was used as a protein loading control. The relative protein expression was quantified by densitometry and normalized to ACTB. All data are shown as means ± S.D. **B** Oil Red O staining analysis in porcine subcutaneous fat preadipocytes (PFs) transfected with shCTL and sh*NSUN2* adenovirus. Scale bar: 100 µm. **C** qRT-PCR analysis in porcine subcutaneous fat preadipocytes (PFs) transfected with shCTL and sh*NSUN2* adenovirus. 18S rRNA served as an internal RNA control. Error bars represent means ± SD; *n* = 3. **D** Western blotting analysis in PFs transfected with control (Vector), NSUN2-WT and NSUN2-MUT adenovirus. ACTB was used as a protein loading control. The relative protein expression was quantified by densitometry and normalized to ACTB. All data are shown as means ± S.D. **E** Oil Red O staining analysis in PFs transfected with control (Vector), NSUN2-WT and NSUN2-MUT adenovirus. Scale bar: 100 µm. **F** qRT-PCR analysis in PFs transfected with control (Vector), NSUN2-WT and NSUN2-MUT adenovirus. 18S rRNA served as an internal RNA control. Error bars represent means ± SD; *n* = 3. **G** Western blotting analysis in porcine muscle satellite cells (SCs) transfected with shCTL or sh*NSUN2*. ACTB was used as a protein loading control. The relative protein expression was quantified by densitometry and normalized to ACTB. All data are shown as means ± S.D. **H** Phase images analysis in porcine muscle satellite cells (SCs) transfected with shCTL or sh*NSUN2*. Scale bar: 100 µm. **I** qRT-PCR analysis in porcine muscle satellite cells (SCs) transfected with shCTL or sh*NSUN2*. 18S rRNA served as an internal RNA control. Error bars represent means ± SD; *n* = 3. **J** Western blotting analysis in SCs transfected with control (Vector), NSUN2-WT and NSUN2-MUT adenovirus. ACTB was used as a protein loading control. The relative protein expression was quantified by densitometry and normalized to ACTB. All data are shown as means ± S.D. **K** Phase images analysis in SCs transfected with control (Vector), NSUN2-WT and NSUN2-MUT adenovirus. Scale bar: 100 µm. **L** qRT-PCR analysis in SCs transfected with control (Vector), NSUN2-WT and NSUN2-MUT adenovirus. 18S rRNA served as an internal RNA control. Error bars represent means ± SD; *n* = 3. The *p* values were determined using Student's *t* tests. *P < 0.05 **P < 0.01, ***P < 0.001

than J and YJ. However, the body fat ratio, average back fat thickness and intramuscular fat ratio of Y were significantly lower than those of J. These fatness-related characters of YJ were just between the two breeds of Y and J (Fig. 1C).

m^{5}C has been shown to be closely related to energy metabolism [15]. Therefore, we measured m^{5}C abundance in BL and LDM from three pig breeds by liquid chromatography–tandem mass spectrometry (LC–MS/MS) to explore the potential relationship between m^{5}C and fatness/muscle growth. We observed that the ratio of m^{5}C/C in total mRNA from the BL and LDM of the three breeds ranged from 0.1 to 0.4%, and a statistically significant higher m^{5}C level was found both in BL and LDM of Y compared to J or YJ (Fig. 1D). Since NSUN2 was identified as the main m^{5}C methyltransferase of mRNA in many species including human and mouse [27], we analyzed its mRNA and protein expressions in BL and LDM from the three pig breeds. The results suggest that NSUN2 mRNA and protein expression

levels were much higher both in BL and LDM of Y compared to J or YJ (Fig. 1E, F). These results indicate that higher m^{5}C levels in mRNA may be associated with lower fat mass, and higher muscle mass in pigs, due to intrinsic genetic, or epigenetic differences between the pig breeds.

Distribution of mRNA m⁵C in BL and LDM from three pig breeds

For a comprehensive overview of a transcriptome-wide landscape of m^{5}C profiles at single-base pair resolution, we performed an improved RNA bisulfite sequencing (RNA-Bis-Seq) analysis on RNA samples purified from adipose tissue (backfat layer, BL) and skeletal muscle (*longissimus dorsi* muscles, LDM) of three pig breeds as previously described [8]. To ensure the efficiency of bisulfite-mediated C to T conversion, the threshold for global conversion rate (C–T) was set to > 99% using *Dhfr* control (Table S4). The results were highly reproducible between independent replicates (Fig. S1A–D). Thus, our approach was considered successful for identifying m^{5}C sites in transcriptomes.

The m^{5}C distribution of mRNA in distinct regions (5′ untranslated region, 5′UTR; coding sequences, CDS; 3′ untranslated region, 3′UTR) showed that the majority of m^{5}C sites was found to be in CDS ranging from 45 to 60% in BL and LDM of Y, YJ, and J (Fig. 2A). A total of 8 384, 7 615, and 6 950 m^{5}C sites within 1 127, 1 118, 1 261 mRNAs were identified in BL from Y, YJ and J, respectively (Fig. 2B, Table S5). A total of 5 430, 6 925, and 5 287 m^{5}C sites within 761, 926, 819 mRNAs were identified in LDM from Y, YJ and J, respectively (Fig. 2B, Table S5). Notably, the median m^{5}C level of mRNA was about 20% in all samples (Fig. 2C). Interestingly, sequence frequency logo analysis demonstrated that the majority of mRNA m^{5}C sites were in CG-rich environments (Fig. 2D). Next, we determined the distribution pattern of m^{5}C sites along mRNA transcripts, and m^{5}C sites showed an enrichment in CDS regions immediately downstream of the translation initiation sites (Fig. 2E). These results are consistent to recently published studies from humans and mice [8], suggesting that highly conserved features not only exist in multiple species, but are observed in pig adipose and muscle tissues. To further validate our results from the RNA-BisSeq analysis, five m^{5}C-modified genes were randomly selected to perform m^{5}C meRIP-qPCR. We observed a significant m^{5}C enrichment of all the five candidates over the IgG control (Fig. 2F).

Taken together, using the stringent m^{5}C calling parameters and the alternative method, our RNA-BisSeq results allow a reliable picture of the mRNA m^{5}C epi-transcriptome in adipose tissue and skeletal muscles of the three pig breeds.
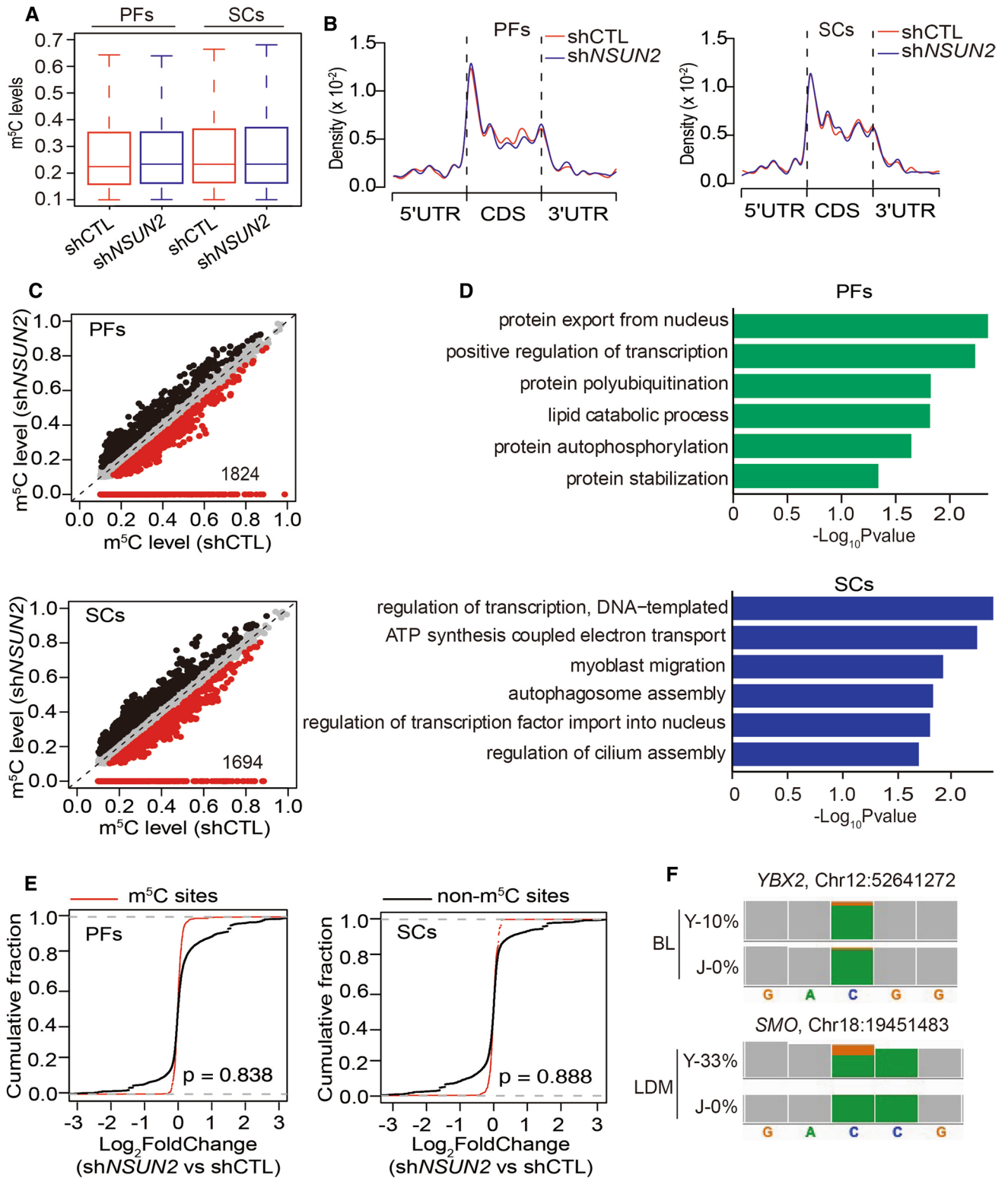
A (PFs, SCs) m5C levels boxplots comparing shCTL and shNSUN2

B Density distribution across 5'UTR, CDS, 3'UTR for PFs and SCs (shCTL red, shNSUN2 blue)

C m5C level scatter plots (shNSUN2 vs shCTL) for PFs (1824) and SCs (1694)

D GO term bar charts of -Log$_{10}$Pvalue for PFs and SCs:

PFs:
- protein export from nucleus
- positive regulation of transcription
- protein polyubiquitination
- lipid catabolic process
- protein autophosphorylation
- protein stabilization

SCs:
- regulation of transcription, DNA−templated
- ATP synthesis coupled electron transport
- myoblast migration
- autophagosome assembly
- regulation of transcription factor import into nucleus
- regulation of cilium assembly

E Cumulative fraction vs Log$_2$FoldChange (shNSUN2 vs shCTL); m5C sites and non-m5C sites; PFs p = 0.838, SCs p = 0.888

F YBX2, Chr12:52641272 (BL: Y-10%, J-0%); SMO, Chr18:19451483 (LDM: Y-33%, J-0%)

◄**Fig. 5** YBX2 and SMO are the potential m^{5}C targets for the regulation of adipogenesis and myogenesis. **A** Boxplots showing the overall distributions of mRNA m^{5}C levels in PFs and SCs with or without *NSUN2* knockdown. **B** Transcriptome-wide distribution pattern of mRNA m^{5}C sites within distinct mRNA regions (5'UTR, CDS and 3'UTR) in PFs and SCs with or without *NSUN2* knockdown. **C** Scatter plot showing m^{5}C levels in PFs and SCs with or without *NSUN2* knockdown. For m^{5}C sites in shCTL PFs, sites with increased or reduced methylation levels depending on *NSUN2* knockdown highlighted in black or red color. **D** Bar plot showing the result of GO analysis of mRNAs with differentially expressed m^{5}C sites in PFs and SCs with or without *NSUN2* knockdown. **E** Cumulative distribution analysis of the expression level changes in mRNAs with or without m^{5}C modification in PFs and SCs. **F** Genome browser view of differentially methylated genes, *YBX2* and *SMO*, in BL or LDM between Y and J by Integrative Genomics Viewer (IGV). The orange boxes indicate methylated cytosine. The green boxes indicate non-methylated cytosine. The proportion of orange in column represents m^{5}C level in *YBX2* or *SMO*

Hypermethylated m^{5}C in B Land LDM strongly relate to fatness/growth-related phenotypes

To explore the relationship between m^{5}C and fatness/growth-related phenotypes between breeds, we performed a principal component analysis (PCA) based on all m^{5}C sites identified by RNA-BisSeq. The result suggest that the samples were clustered into the BL and LDM group, indicating the potentially specific roles of m^{5}C in different tissues (Fig. 3A). Next, we combined all m^{5}C-modified genes in BL or LDM from the three breeds and performed KEGG pathway enrichment analysis. The m^{5}C-containing genes in BL were clearly involved in the lipid metabolism-related pathways during adipogenesis, such as insulin signaling, ECM receptor, MAPK signaling, mTOR signaling, VEGF signaling and PPAR (Fig. 3B). In LDM, m^{5}C-containing genes were involved in MAPK signaling, VEGF receptor, and mTOR signaling, Aldosterone synthesis and secretion, AMPK signaling and the Wnt signaling pathway (Fig. 3B), which are closely linked to myogenesis. These results suggest that m^{5}C may play an important role for accounting for phenotype differences in BL or LDM between the three breeds pigs. As significant phenotypic differences are observed between Y and J, the significantly different m^{5}C sites were screened in BL or LDM from Y and J and were subjected to hierarchical cluster analysis. The m^{5}C site levels in BL or LDM showed big differences between Y and J (Fig. 3C). More importantly, the phenotypic parameters of YJ ranked intermediate among the three pig breeds (Fig. 1B, C), and the m^{5}C site levels in BL or LDM from YJ were also intermediate (Fig. 3C), implying that these different m^{5}C sites were strongly related to fatness/growth-related phenotypes.

Next, we explored the underlying function of different m^{5}C sites in BL or LDM. Since total mRNA m^{5}C levels in BL or LDM were significantly higher in Y compared with J

(Fig. 1D), genes with higher m^{5}C site levels in Y than J were selected and subjected to KEGG analysis. We observed that hypermethylated genes in BL and LDM were significantly enriched in signaling pathways linked to impaired adipogenesis and enhanced myogenesis (Fig. 3D), indicating that m^{5}C negatively can regulate fat deposition and positively affects muscle differentiation. Besides, hypomethylated genes in BL and LDM were related to pathways, such as metabolic pathways and mTOR signaling (Fig. S1E), indicating that mRNA m^{5}C may play an important role in metabolic regulation. To identify the function of m^{5}C in our study, we performed RNA-seq of BL and LDM in the three breeds (Table S6). When comparing RNA abundance between m^{5}C-modified and non-m^{5}C-modified mRNAs in BL and LDM between Y and J, no significant correlation between mRNA abundance and m^{5}C levels was observed (Fig. 3E), suggesting that m^{5}C may not influenced adipose and muscle development by maintaining mRNAs expression.

Taken together, our hypothesis that m^{5}C contributes to the fatness/growth-related phenotype in pigs, suggests that it has an important mechanistic role in adipogenesis and myogenesis.

m^{5}C inhibits adipogenesis in PFs and promotes myogenesis in SCs

Since NSUN2 was identified as the main mRNA m^{5}C methyltransferase in many species [27], NSUN2 was used to manipulate the m^{5}C level in our study. Expectedly, knockdown of NSUN2 significantly decreased the m^{5}C level (Fig. S2A). Next, we constructed wild-type and mutant NSUN2 (C274A/C324A) adenovirus plasmids (NSUN2-WT, NSUN2-MUT) by changing the m^{5}C methyltransferase activity based on published work [8]. HPLC–MS/MS results show that overexpressing NSUN2-WT could significantly increase mRNA m^{5}C levels, but overexpressing NSUN2-MUT did not affect mRNA m^{5}C levels (Fig. S2B).

To explore the role of m^{5}C in regulating adipogenesis, PFs were isolated from BL. In PFs, decreasing m^{5}C levels by silencing NSUN2 significantly enhanced lipid accumulation and mRNA expression of adipogenic transcription factors including peroxisome proliferator activated receptor gamma (*PPARG*), fatty acid binding protein 4 (*FABP4*) and CCAAT/enhancer binding protein alpha (*C/EBPA*) (Fig. 4A–C). Increasing m^{5}C levels by overexpressing of NSUN2-WT (rather than NSUN2-MUT) impaired PFs adipogenic differentiation and inhibited expression of P*PARG* , *FABP4* and *C/EBPA* (Fig. 4D–F). Porcine muscle satellite cells (SCs) were isolated from LDM to investigate the role of m^{5}C in regulating myogenesis. In SCs, decreasing m^{5}C levels by silencing *NSUN2* impaired protein expression of myosin heavy chain 1 (MYH1) and the mRNA expression of the myogenic differentiation marker gene creatine kinase
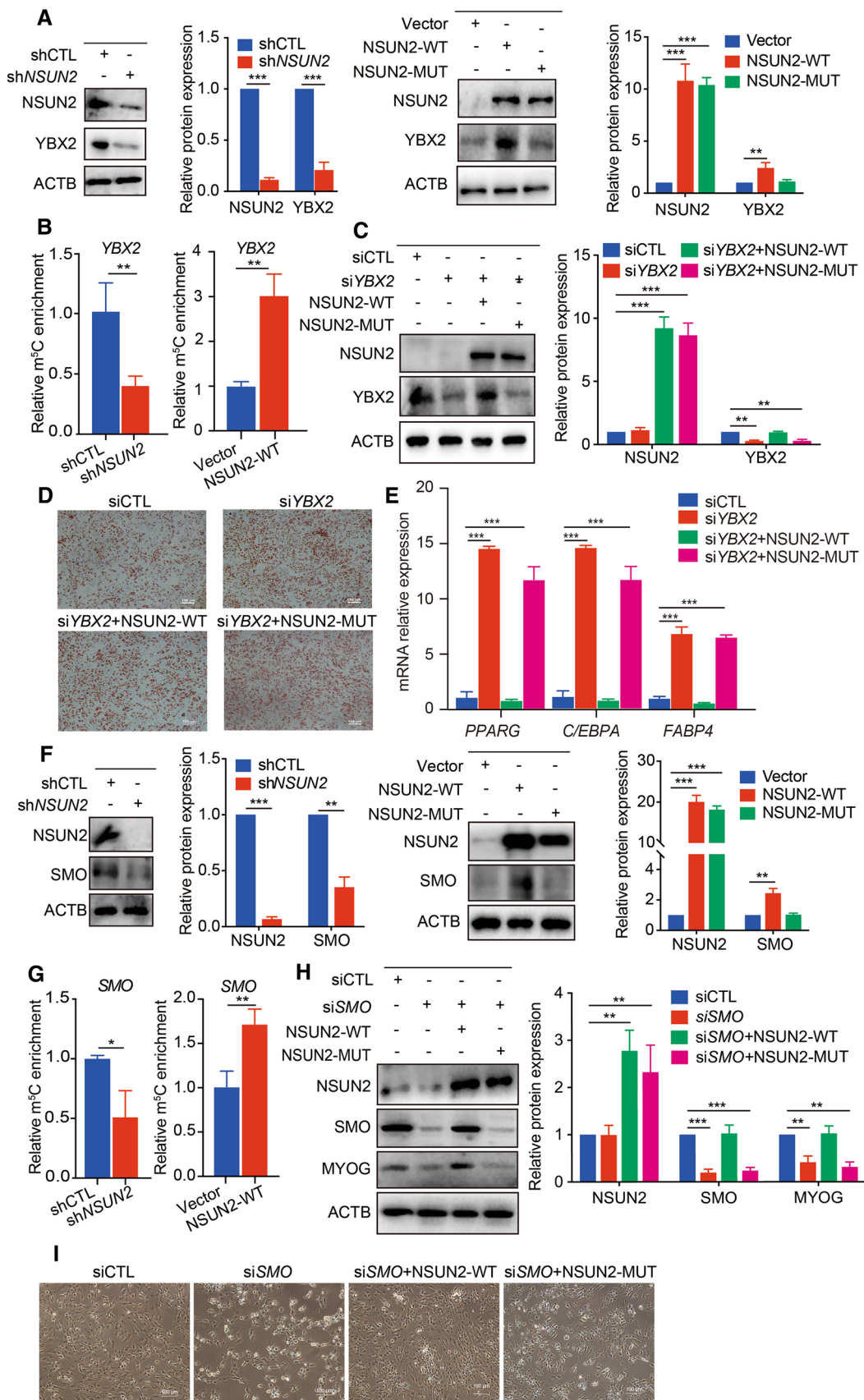
◀**Fig. 6** YBX2 and SMO inhibit adipogenesis and promote myogenesis in m^{5}C-dependent manner. **A** Western blotting of NSUN2 and YBX2 expression in PFs transfected with shCTL, sh*NSUN2*, vector, NSUN2-WT or NSUN2-MUT adenovirus. ACTB was used as a loading control. The relative protein expression was quantified by densitometry and normalized to ACTB. All data are shown as means ± S.D. **B** m^{5}C-RIP-qPCR analysis of *YBX2* in PFs transfected with shCTL, sh*NSUN2*, Vector or NSUN2-WT adenovirus. Error bars, means ± S.D., *n* = 3. **C** Western blotting analysis in control or *YBX2* knockdown PFs transfected with NSUN2-WT or NSUN2-MUT adenovirus. ACTB was used as a protein loading control. The relative protein expression was quantified by densitometry and normalized to ACTB. All data are shown as means ± S.D. **D** Oil Red O staining analysis in control or *YBX2* knockdown PFs transfected with NSUN2-WT or NSUN2-MUT adenovirus. Scale bar: 100 μm. **E** qPCR analysis in control or *YBX2* knockdown PFs transfected with NSUN2-WT or NSUN2-MUT adenovirus. 18S rRNA served as an internal RNA control. Error bars represent means ± SD; *n* = 3. **F** Western blotting of NSUN2 and SMO expression in SCs transfected with shCTL, sh*NSUN2*, Vector, NSUN2-WT or NUSN2-MUT adenovirus. ACTB was used as a loading control. The relative protein expression was quantified by densitometry and normalized to ACTB. All data are shown as means ± S.D. **G** m^{5}C-RIP-qPCR analysis of *SMO* in SCs transfected with shCTL, sh*NSUN2*, Vector or NSUN2-WT adenovirus. Error bars, means ± S.D., *n* = 3. **H** Western blotting in control or SMO knockdown SCs transfected with NSUN2-WT or NSUN2-MUT adenovirus. ACTB was used as a protein loading control. The relative protein expression was quantified by densitometry and normalized to ACTB. All data are shown as means ± S.D. **I** Phase image in control or *SMO* knockdown SCs transfected with NSUN2-WT or NSUN2-MUT adenovirus. Scale bar: 100 μm. The *P* values were determined using Student's *t* tests. *P < 0.05 **P < 0.01, ***P < 0.001

M-type (*CKM*) (Fig. 4G–I). Expectedly, only increasing m^{5}C levels by overexpressing NSUN2-WT rather than NSUN2-MUT could promote myogenesis in SCs (Fig. 4J–L), indicating that m^{5}C triggers myogenesis. Thus, m^{5}C blocked adipogenesis and up- regulated myogenesis.

YBX2 and SMO are the potential m^{5}C targets for the regulation of adipogenesis and myogenesis

To uncover the underlying mechanism of m^{5}C in adipogenesis and myogenesis, RNA-BisSeq and RNA-seq were conducted in PFs and SCs with or without knocking down of *NSUN2*. Only candidate m^{5}C sites present in two replicates were used for further analyses (Fig. S3A, B, Table S7, 8). It is worth noting that median m^{5}C levels (Fig. 5A) and distribution patterns of m^{5}C sites in PFs and SCs (Fig. 5B) were similar in BL or LDM (Fig. 2C, E). When we identified 1824 and 1694 m^{5}C sites with methylation levels reduction upon NSUN2 knockdown in PFs and SCs (Fig. 5C), we observed almost the same result as in humans[8], suggesting that knockdown of *NSUN2* could significantly reduce the mRNA m^{5}C level in PFs or SCs.

Next, enrichment analysis was performed to illustrate the potential function of m^{5}C in *NSUN2*-knocked-down cells. In PFs with *NSUN2* knockdown, the differentially m^{5}C-modified genes were significantly enriched in lipid catabolic processes which negatively correlated with adipogenesis (Fig. 5D). The differentially m^{5}C-modified genes in *NSUN2*-knocked-down SCs were linked to myoblast migration which was essential for myogenesis (Fig. 5D). Interestingly, consistent with the tissue findings outlined above (Fig. 3E), depending on silencing of *NSUN2*, no significant RNA abundance changes were found between m^{5}C-modified and non-m^{5}C-modified mRNAs in PFs and SCs (Fig. 5E, Tables S9, S10), suggesting that m^{5}C indeed regulated adipogenesis and myogenesis not by stabilizing mRNAs. Subsequently, to figure out potential m^{5}C targets for the regulation of adipogenesis and myogenesis, we combined the RNA-BisSeq results from both tissues and cell data. *YBX2* and *SMO* were then ruled out as potential m^{5}C targets for the regulation of adipogenesis and myogenesis. The methylation level of *YBX2* and *SMO* was higher in BL and LDM of Y compared with J (Fig. 5F).

Together, our results suggest that m^{5}C regulation during inhibition of adipogenesis and promotion of myogenesis may occur through controlling lipid catabolism and myoblast migration via YBX2 and SMO.

YBX2 and SMO inhibit adipogenesis and promote myogenesis in m^{5}C-dependent manner

YBX2 belongs to the YBX family which is mainly involved in RNA binding, transcription and translation, and was previously reported to be required for cold-induced brown adipose tissue activation, which strongly relates to lipid catabolism [28]. It is worth noting that the protein levels of YBX2 decreased when NSUN2 was inhibited, and overexpression of NSUN2-WT rather than NSUN2-MUT could promote the expression of YBX2 (Fig. 6A). Besides, meRIP-qPCR results showed that silencing *NSUN2* significantly decreased m^{5}C level of *YBX2* mRNA, while overexpression of NSUN2 increased the m^{5}C level of *YBX2* mRNA (Fig. 6B), suggesting that *YBX2* was indeed affected in an m^{5}C-dependent manner. Then, *YBX2* was blocked using *YBX2* siRNA during adipogenesis. We observed an aggravated lipid accumulation and increased mRNA expression of *PPARG*, *C/EBPA* and *FABP4* in *YBX2* knockdown PFs (Fig. 6C–E and Fig. S4A), which was consistent with the results in *NSUN2*-silenced PFs (Fig. 4A, B). More importantly, the enhanced adipogenesis in *YBX2* knocked-down PFs could be reversed by transfection with NSUN2-WT rather than NSUN2-MUT
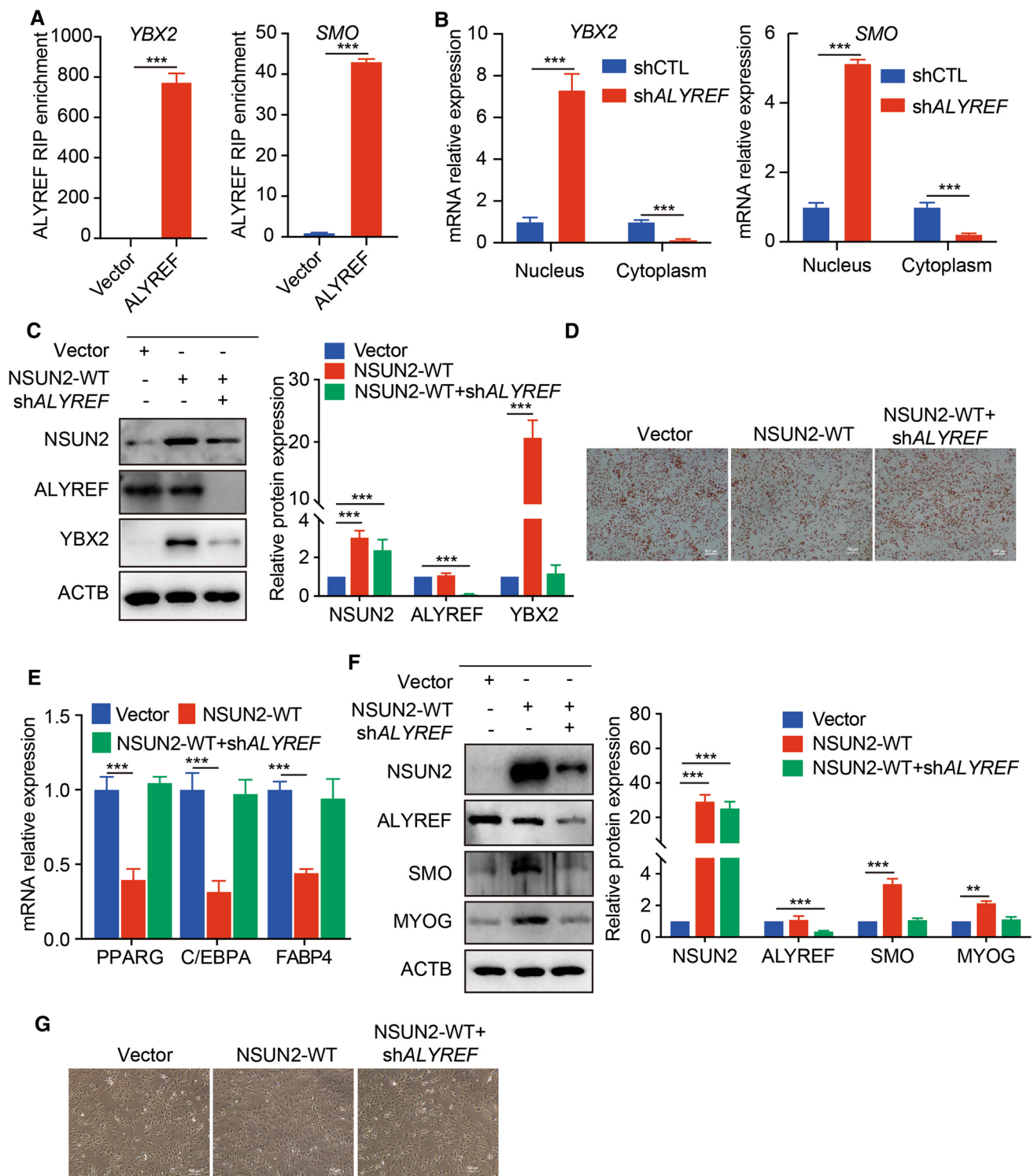
(Fig. 6C–E and Fig. S4A). These findings demonstrate that m^{5}C inhibited lipid accumulation by targeting *YBX2*.

As a G protein-coupled receptor, SMO reportedly participates in myoblast migration and skeletal muscle development [29]. Deletion of *NSUN2* blocked protein expression of SMO in SCs, while only overexpression of NSUN2-WT rather than NSUN2-MUT increased the SMO protein level (Fig. 6F). In addition, meRIP-qPCR showed that *SMO* mRNA could be dynamically methylated by silencing or overexpressing NSUN2 (Fig. 6G), suggesting that m^{5}C was required for the regulation of SMO expression. To investigate the role of the candidate gene for myogenesis, we

◄**Fig. 7** The role of YBX2 and SMO was mediated by ALYREF in a m^{5}C-dependent manner. **A** RIP-qPCR analysis of *YBX2* in PFs (left) and SCs (right) transfected with vector or ALYREF-Flag adenovirus. Error bars, means ± S.D., $n = 3$. **B** qPCR analysis of *YBX2* and *SMO* mRNA in the nucleus or cytoplasm of control and *ALYREF* knockdown PF and SCs respectively. 18S rRNA served as an internal RNA control. Error bars represent means ± SD; $n = 3$. **C** Western blotting analysis in control or NSUN2-WT overexpressing PFs transfected with or without sh*ALYREF* adenovirus. ACTB was used as a protein loading control. The relative protein expression was quantified by densitometry and normalized to ACTB. All data are shown as means ± S.D. **D** Oil Red O staining analysis in control or NSUN2-WT overexpressing PFs transfected with or without sh*ALYREF* adenovirus. Scale bar: 100 μm. **E** qPCR analysis in control or NSUN2-WT overexpressing PFs transfected with or without sh*ALYREF* adenovirus. 18S rRNA served as an internal RNA control. Error bars represent means ± SD; $n = 3$. **F** Western blotting in control or NSUN2-WT overexpressing SCs transfected with or without sh*ALYREF* adenovirus. ACTB was used as a protein loading control. The relative protein expression was quantified by densitometry and normalized to ACTB. All data are shown as means ± S.D. **G** Phase image in control or NSUN2-WT overexpressing SCs transfected with or without sh*ALYREF* adenovirus. Scale bar: 100 μm. The *P* values were determined using Student's *t* tests. *$P < 0.05$ **$P < 0.01$, ***$P < 0.001$

knocked down *SMO* and observed decreased expression of myogenin (MYOG) and a sharp decline in cell number (Fig. 6H, I and Fig. S4B). More importantly, the blocked expression of MYOG and myogenesis in *SMO* knocked-down SCs could be rescued by upregulating NSUN2-WT rather than NSUN2-MUT (Fig. 6H, I and Fig. S4B). Thus, m^{5}C promoted myogenesis through targeting *SMO*.

The role of YBX2 and SMO was mediated by ALYREF in a m⁵C-dependent manner

Generally, m^{5}C need to be recognized by its readers, Y-box-binding protein 1 (YBX1) or ALYREF, to exert a specific role for regulating mRNA stability and mRNA export [8, 14]. As the m^{5}C modification did not affect mRNA levels of *YBX2* and *SMO*, we examined whether ALYREF was the potential reader in controlling adipogenesis and myogenesis. To test this hypothesis, we performed RIP-qPCR analysis around the m^{5}C sites and observed a significant enrichment of *YBX2* and *SMO* in ALYREF-flag overexpressing cells (Fig. 7A). ALYREF could directly bind to *YBX2* and *SMO* mRNA by recognizing m^{5}C modification. Next, nucleus and cytoplasm RNAs were isolated to determine *YBX2/SMO* mRNAs subcellular location mediated by ALYREF. qPCR analysis revealed that the majority of mRNAs of *YBX2* or *SMO* were accumulated in the nucleus when *ALYREF* was inhibited (Fig. 7B), suggesting that ALYREF served indeed as reader for the binding to *YBX2* and *SMO* to regulate mRNA export. Functionally, increased YBX2 expression, decreased mRNA expression of adipogenic differentiation marker genes and reduced lipid accumulation

in NSUN2-WT overexpressing PFs could be rescued by silencing of *ALYREF* (Fig. 7C–E and Fig. S4C). Knockdown of *ALYREF* could reverse the augmented expression of SMO and MYOG and reinforcement of myogenesis when NSUN2-WT was overexpressed in SCs (Fig. 7F, G and Fig. S4D). Taken together, m^{5}C inhibited adipogenesis and promoted myogenesis through ALYREF-m^{5}C-*YBX2* and ALYREF-m^{5}C-*SMO*.

Discussion

Previous studies indicated that m^{5}C is involved in various biological processes, including oxidative stress, adaptation to high temperatures, germ line stem cell development, maternal-to-zygotic transition and tumorigenesis, all by modulating mRNA subcellular localization, stability and translation [8, 11–14, 30, 31]. We found that m^{5}C may play a critical role in tissue-specific functions including lipid metabolism and muscle development. We demonstrated that hypermethylated genes in BL and LDM were linked to reduced adipogenesis and enhanced myogenesis. NSUN2 was identified as the main m^{5}C methyltransferase of mRNA in eukaryotes [8]. NSUN2-mediated m^{5}C could control cell cycle progression via modulating cyclin-dependent kinase 1 (CDK1) and cyclin-dependent kinase inhibitor 1A (CDKN1A) translation in human cells [32, 33]. Moreover, reduction of m^{5}C by depleting *NSUN2* caused disturbed neuron differentiation and migration of neuroepithelial progenitors during brain development, resulting in Dubowitz-like syndrome [34]. Interestingly, it was demonstrated that the depletion of transcription factor MSX2 suppressed the transcription of *NSUN2* [35]. In this study, we found that *NSUN2* mRNA was much higher both in BL and LDM of Y compared to J or YJ, leading us to speculate that there may be some transcription factors that can regulate *NSUN2* transcription in different pig breeds. In our study, we demonstrated that knockdown of *NSUN2* could significantly reduce the mRNA m^{5}C level in PFs or SCs. In addition to in vitro assays, we performed *NSUN2* knockdown or overexpression assays to manipulate the mRNA m^{5}C levels and we found that m^{5}C inhibited adipogenesis and promoted myogenesis.

From the RNA-BisSeq data, we found that hypermethylated genes in BL and LDM were related to impaired adipogenesis and enhanced myogenesis. It was worth noting that the methylation level of *YBX2* and *SMO* was higher in BL and LDM of Y compared with J, which was consistent with the RNA-BisSeq data from tissues, promoting us to explore the function of these two gene in pigs. It was observed that YBX2 is involved in the biological process of tumorigenesis, including human testicular seminoma and ovarian asexual germ cell tumor and oral squamous cell carcinoma [36, 37].

Besides, YBX2 was found to be enriched in BAT to target and maintain PPAR GC1A RNA stability during cold-induced brown fat activation [28]. In our study, we found that NSUN2-mediated m^{5}C inhibition of adipogenesis by increasing YBX2 protein expression. However, whether YBX2 could regulate mitochondrial function and lipolysis via stabilizing *PPARGC1A* or other mRNAs will have to be answered in future experiments. As key regulator for fate determination of embryonic stem cells, Hedgehog signaling activation was frequently observed in development and tumorigenesis [38, 39]. SMO, the key component of Hedgehog signaling [40], was reported to promote myogenic proliferation and differentiation via the MAPK/ERK and PI3K/Akt pathway [29]. We observed restrained cell proliferation and differentiation of SCs during transfection with *SMO* siRNA. More importantly, the inhibitory effect in *SMO* knocked-down SCs could be rescued by overexpressing of NSUN2-WT, suggesting that the m^{5}C-*SMO*-Hedgehog signaling axis may play a critical regulatory role during myogenesis or muscle development.

Similar to m^{6}A, m^{5}C readers, including ALYREF and YBX1, were required to recognize m^{5}C modification in mRNA to exert its regulatory function. There is experimental evidence that ALYREF contributes to promoting mRNA export of m5c-containing mRNA [41]. Different from ALYREF, YBX1, a cytoplasmic mRNA m^{5}C reader, regulates mRNA stability in the fruit fly, human and zebrafish [13, 14]. In our work, we could not confirm a significant difference in RNA abundance between m^{5}C-modified and non-m^{5}C-modified mRNA in vivo and in vitro. Presumably, m^{5}C modification generally had no effect on mRNA stabilization in the development of adipose tissue and skeletal muscle. Rather, ALYREF was identified as m^{5}C reader, regulating adipogenesis and myogenesis by promoting *YBX2* and *SMO* mRNA export. In conclusion, we describe a novel mechanism of mRNA m^{5}C-mediated inhibition of adipogenesis and improved myogenesis. *YBX2* and *SMO* with higher m^{5}C were recognized and exported to cytoplasm from nucleus by ALYREF leading to increased YBX2 and SMO protein expression, thereby inhibiting adipogenesis and promoting myogenesis respectively. Although pigs are very similar to humans, it is necessary to verify the function of mRNA m^{5}C in human tissues. As we known, the RNA m^{5}C machinery is complex, thus further investigation focusing on systematic study of the underlying regulatory network of m^{5}C-modified genes would provide significant opportunity to get insight into the coordination between mRNA m^{5}C metabolism and adipose tissue or skeletal muscle development. Our work provides a valuable resource for deciphering the function of mRNA m^{5}C modification in the emergence of fatness and diseases relating to skeletal muscle dysfunction.

Conclusion

We discovered a novel mechanism of mRNA m^{5}C-mediated inhibition of adipogenesis and advancement of myogenesis. *YBX2* and *SMO* with higher m^{5}C are recognized and exported to the cytoplasm from the nucleus by ALYREF leading to increased YBX2 and SMO protein expression, thereby inhibiting adipogenesis and promoting myogenesis respectively.

Declarations

Conflict of interest The authors declare no conflict of interest.

Ethical statement Sample collection in this study was performed according to the guidelines for the care and use of experimental animals established by the Ministry of Agriculture of China. All procedures were approved by the Committee on Animal Care and Use and Committee on the Ethics of Animal Experiments of Zhejiang University (ZJU2015-458-09).

References

1. Goodpaster BH, Sparks LM (2017) Metabolic flexibility in health and disease. Cell Metab 5(25):1027–1036. https://doi.org/10.1016/j.cmet.2017.04.015
2. Ukropec J, Ukropcova B, Kurdiova T, Gasperikova D, Klimes I (2008) Adipose tissue and skeletal muscle plasticity modulates metabolic health. Arch Physiol Biochem 5(114):357–368. https://doi.org/10.1080/13813450802535812
3. Tidball JG (2017) Regulation of muscle growth and regeneration by the immune system. Nat Rev Immunol 3(17):165–178. https://doi.org/10.1038/nri.2016.150
4. Yang S, Yang G, Wu H, Kang L, Xiang J, Zheng P et al (2021) MicroRNA-193b impairs muscle growth in mouse models of type 2 diabetes by targeting the PDK1/Akt signalling pathway. Diabetologia. https://doi.org/10.1007/s00125-021-05616-y
5. Petersen MC, Shulman GI (2018) Mechanisms of insulin action and insulin resistance. Physiol Rev 4(98):2133–2223. https://doi.org/10.1152/physrev.00063.2017
6. Zhao BS, Roundtree IA, He C (2017) Post-transcriptional gene regulation by mRNA modifications. Nat Rev Mol Cell Biol 1(18):31–42. https://doi.org/10.1038/nrm.2016.132
7. Wu R, Wang X (2020) Epigenetic regulation of adipose tissue expansion and adipogenesis by *N*(6) -methyladenosine. Obesity Rev. https://doi.org/10.1111/obr.13124
8. Yang X, Yang Y, Sun BF, Chen YS, Xu JW, Lai WY et al (2017) 5-methylcytosine promotes mRNA export - NSUN2 as the methyltransferase and ALYREF as an m(5)C reader. Cell Res 5(27):606–625. https://doi.org/10.1038/cr.2017.55
9. Liu RJ, Long T, Li J, Li H, Wang ED (2017) Structural basis for substrate binding and catalytic mechanism of a human RNA:m5C methyltransferase NSun6. Nucleic Acids Res 11(45):6684–6697. https://doi.org/10.1093/nar/gkx473
10. Selmi T, Hussain S, Dietmann S, Heiss M, Borland K, Flad S et al (2021) Sequence- and structure-specific cytosine-5 mRNA methylation by NSUN6. Nucleic Acids Res 2(49):1006–1022. https://doi.org/10.1093/nar/gkaa1193
11. Tang Y, Gao CC, Gao Y, Yang Y, Shi B, Yu JL et al (2020) OsNSUN2-mediated 5-methylcytosine mRNA modification enhances rice adaptation to high temperature. Dev Cell 3(53):272–286. https://doi.org/10.1016/j.devcel.2020.03.009 (**e7**)
12. Zou F, Tu R, Duan B, Yang Z, Ping Z, Song X et al (2020) Drosophila YBX1 homolog YPS promotes ovarian germ line stem cell development by preferentially recognizing 5-methylcytosine RNAs. Proc Natl Acad Sci USA 7(117):3603–3609. https://doi.org/10.1073/pnas.1910862117
13. Chen X, Li A, Sun BF, Yang Y, Han YN, Yuan X et al (2019) 5-methylcytosine promotes pathogenesis of bladder cancer through stabilizing mRNAs. Nat Cell Biol 8(21):978–990. https://doi.org/10.1038/s41556-019-0361-y
14. Yang Y, Wang L, Han X, Yang WL, Zhang M, Ma HL et al (2019) RNA 5-methylcytosine facilitates the maternal-to-zygotic transition by preventing maternal mRNA decay. Mol Cell 6(75):1188–1202. https://doi.org/10.1016/j.molcel.2019.06.033 (**e11**)
15. Van Haute L, Lee SY, McCann BJ, Powell CA, Bansal D, Vasiliauskaite L et al (2019) NSUN2 introduces 5-methylcytosines in mammalian mitochondrial tRNAs. Nucleic Acids Res 16(47):8720–8733. https://doi.org/10.1093/nar/gkz559
16. Moretti A, Fonteyne L, Giesert F, Hoppmann P, Meier AB, Bozoglu T et al (2020) Somatic gene editing ameliorates skeletal and cardiac muscle failure in pig and human models of Duchenne muscular dystrophy. Nat Med 2(26):207–214. https://doi.org/10.1038/s41591-019-0738-2
17. Koopmans SJ, Schuurman T (2015) Considerations on pig models for appetite, metabolic syndrome and obese type 2 diabetes: from food intake to metabolic disease. Eur J Pharmacol 759:231–239. https://doi.org/10.1016/j.ejphar.2015.03.044
18. Miao Z, Wang S, Wang Y, Wei P, Khan MA, Zhang J et al (2019) Comparison of microRNAs in the intramuscular adipose tissue from Jinhua and Landrace pigs. J Cell Biochem 1(120):192–200. https://doi.org/10.1002/jcb.27298
19. Wang X, Sun B, Jiang Q, Wu R, Cai M, Yao Y et al (2018) mRNA m(6)A plays opposite role in regulating UCP2 and PNPLA2 protein expression in adipocytes. Int J Obes (Lond) 11(42):1912–1924. https://doi.org/10.1038/s41366-018-0027-z
20. Jiang Q, Sun B, Liu Q, Cai M, Wu R, Wang F et al (2019) MTCH2 promotes adipogenesis in intramuscular preadipocytes via an m(6)A-YTHDF1-dependent mechanism. FASEB J 2(33):2971–2981. https://doi.org/10.1096/fj.201801393RRR
21. Wang J, Xiao J, Liu X, Gao Y, Luo Z, Gu X et al (2021) Tandem mass tag-labeled quantitative proteomic analysis of tenderloins between Tibetan and Yorkshire pigs. Meat Sci 172:108343. https://doi.org/10.1016/j.meatsci.2020.108343
22. Zhang W, Chen Q, Xu L, Cai J, Zhang J (2021) The potential role of PSMA6 in modulating fat deposition in pigs by promoting preadipocyte proliferation and differentiation. Gene 769:145228. https://doi.org/10.1016/j.gene.2020.145228
23. Li J, Zhao W, Li Q, Huang Z, Shi G, Li C (2020) Long Noncoding RNA H19 promotes porcine satellite cell differentiation by interacting with TDP43. Genes (Basel). https://doi.org/10.3390/genes11030259
24. Ding S, Wang F, Liu Y, Li S, Zhou G, Hu P (2017) Characterization and isolation of highly purified porcine satellite cells. Cell Death Discov 3:17003. https://doi.org/10.1038/cddiscovery.2017.3
25. Bolger AM, Lohse M, Usadel B (2014) Trimmomatic: a flexible trimmer for Illumina sequence data. Bioinformatics 15(30):2114–2120. https://doi.org/10.1093/bioinformatics/btu170
26. Kim D, Pertea G, Trapnell C, Pimentel H, Kelley R, Salzberg SL (2013) TopHat2: accurate alignment of transcriptomes in the presence of insertions, deletions and gene fusions. Genome Biol 4(14):R36. https://doi.org/10.1186/gb-2013-14-4-r36
27. Chen YS, Yang WL, Zhao YL, Yang YG (2021) Dynamic transcriptomic m(5) C and its regulatory role in RNA processing. Wiley Interdiscip Rev RNA 4(12):e1639. https://doi.org/10.1002/wrna.1639
28. Xu D, Xu S, Kyaw AMM, Lim YC, Chia SY, Chee Siang DT et al (2017) RNA binding protein Ybx2 regulates RNA stability during cold-induced brown fat activation. Diabetes 12(66):2987–3000. https://doi.org/10.2337/db17-0655
29. Madhala-Levy D, Williams VC, Hughes SM, Reshef R, Halevy O (2012) Cooperation between Shh and IGF-I in promoting myogenic proliferation and differentiation via the MAPK/ERK and PI3K/Akt pathways requires Smo activity. J Cell Physiol 4(227):1455–1464. https://doi.org/10.1002/jcp.22861
30. David R, Burgess A, Parker B, Li J, Pulsford K, Sibbritt T et al (2017) Transcriptome-wide mapping of RNA 5-methylcytosine in Arabidopsis mRNAs and noncoding RNAs. Plant Cell 3(29):445–460. https://doi.org/10.1105/tpc.16.00751
31. Amort T, Rieder D, Wille A, Khokhlova-Cubberley D, Riml C, Trixl L et al (2017) Distinct 5-methylcytosine profiles in poly(A)

RNA from mouse embryonic stem cells and brain. Genome Biol 1(18):1. https://doi.org/10.1186/s13059-016-1139-1

32. Xing J, Yi J, Cai X, Tang H, Liu Z, Zhang X et al (2015) NSun2 promotes cell growth via elevating cyclin-dependent kinase 1 translation. Mol Cell Biol 23(35):4043–4052. https://doi.org/10.1128/MCB.00742-15

33. Li Q, Li X, Tang H, Jiang B, Dou Y, Gorospe M et al (2017) NSUN2-mediated m5C methylation and METTL3/METTL14-mediated m6A methylation cooperatively enhance p21 translation. J Cell Biochem 9(118):2587–2598. https://doi.org/10.1002/jcb.25957

34. Flores JV, Cordero-Espinoza L, Oeztuerk-Winder F, Andersson-Rolf A, Selmi T, Blanco S et al (2017) Cytosine-5 RNA methylation regulates neural stem cell differentiation and motility. Stem Cell Reports 1(8):112–124. https://doi.org/10.1016/j.stemcr.2016.11.014

35. He X, Yang Z, Chu XY, Li YX, Zhu B, Huang YX et al (2022) ROR2 downregulation activates the MSX2/NSUN2/p21 regulatory axis and promotes dental pulp stem cell senescence. Stem Cells 3(40):290–302. https://doi.org/10.1093/stmcls/sxab024

36. Niu X, Yang B, Liu F, Fang Q (2020) LncRNA HOXA11-AS promotes OSCC progression by sponging miR-98-5p to upregulate YBX2 expression. Biomed Pharmacother 121:109623. https://doi.org/10.1016/j.biopha.2019.109623

37. Chen F, Liu M, Yu Y, Sun Y, Li J, Hu W et al (2019) LINC00958 regulated miR-627-5p/YBX2 axis to facilitate cell proliferation and migration in oral squamous cell carcinoma. Cancer Biol Ther 9(20):1270–1280. https://doi.org/10.1080/15384047.2019.1617571

38. Wu X, Xiao S, Zhang M, Yang L, Zhong J, Li B et al (2021) A novel protein encoded by circular SMO RNA is essential for Hedgehog signaling activation and glioblastoma tumorigenicity. Genome Biol 1(22):33. https://doi.org/10.1186/s13059-020-02250-6

39. Xiao X, Tang JJ, Peng C, Wang Y, Fu L, Qiu ZP et al (2017) Cholesterol modification of smoothened is required for hedgehog signaling. Mol Cell 1(66):154–162. https://doi.org/10.1016/j.molcel.2017.02.015 (**e10**)

40. Yang C, Zheng X, Ye K, Sun Y, Lu Y, Fan Q et al (2021) Retraction notice to: miR-135a inhibits the invasion and migration of Esophageal cancer stem cells through the hedgehog signaling pathway by targeting Smo. Mol Ther Nucleic Acids 26:1198. https://doi.org/10.1016/j.omtn.2021.09.012

41. Eckwahl M, Xu R, Michalkiewicz J, Zhang W, Patel P, Cai Z et al (2020) 5-Methylcytosine RNA modifications promote retrovirus replication in an ALYREF reader protein-dependent manner. J Virol. https://doi.org/10.1128/JVI.00544-20